RSC Advances

PAPER

View Article Online
View Journal | View Issue

Cite this: *RSC Adv.*, 2026, **16**, 24947

Augmenting the antimicrobial activity of clindamycin hydrochloride-loaded acrylate polymer/zinc oxide nanocomposites against pathogenic microbes

Rokaya A. Sobh, *[a] A. S. Mohammed,[b] W. S. Mohamed,[a] M. K. Zahran[b] and Taha F. Hassanein[b]

Our study's primary goal is to increase clindamycin hydrochloride's antibacterial efficacy by loading it into acrylate polymer/zinc oxide nanocomposites, which is among the most effective ways to accomplish controlled drug release to a precise targeted spot. Zinc oxide nanoparticles (ZnO NPs) were first made at room temperature (25 °C) using starch as a biopolymer stabilizer. The ZnO NPs were produced in almost spheres with an average particle size of 20 ± 2 nm that were verified using transmission electron microscopy (TEM), FT-IR, zeta potential and UV-vis absorbance. Green microemulsion polymerization techniques have been used in the field of polymer manufacturing to create advanced nanocomposites in an environmentally responsible manner. In order to encapsulate clindamycin hydrochloride as a medicinal drug, we have created zinc oxide nanoparticles (ZnO NPs) integrated into polymeric nanospheres made of poly(methyl methacrylate-*co*-hydroxypropyl methacrylate) poly(MMA/HPMA). The prepared drug delivery system is thoroughly characterized *via* morphological and particle size analyzers, zeta potential, FT-IR, and thermal gravimetric analysis (TGA) to study the influence of monomer composition ratio, drug content, and ZnO NP content on the *in vitro* drug release, morphological and structural characteristics, and entrapment efficiency. Well-defined spherical poly(MMA/HPMA) and its nanocomposite with ZnO NPs were created with an average particle size of 31.78 and 50 nm, respectively. It was found that the entrapment efficiency of drugs varied with the ZnO NP ratio and increased, ranging from 62.22 to 82.95% for the polymer nanospheres containing 0 and 5% ZnO NPs, respectively, and confirmed by the transmission electron microscope (TEM) and FTIR spectra. Furthermore, the *in vitro* drug release tests revealed that the drug content and ZnO NPs, as well as the monomer composition ratio, are highly efficient in determining the percentage of drug release. When the HPMA ratio and drug content were higher, it was observed that the drug released more quickly. Otherwise, the drug release was further regulated, delayed, and sustained due to the slower drug release generated by the ZnO NPs in the nanocomposite. The antibacterial activity of the polymer nanocomposite was evaluated based on the zone of inhibition against both Gram-positive and Gram-negative bacteria, and it was shown to be effective against the Gram-positive bacterium *B. subtilis* and the Gram-negative bacterium *E. cloacae* with ZOI (mm) as 34 and 20, respectively.

Received 13th February 2026
Accepted 18th April 2026

DOI: 10.1039/d6ra01292b

rsc.li/rsc-advances

1 Introduction

A nanocomposite is a matrix composed of at least one material with a size between 1 and 100 nm in order to improve the materials' qualities.[1–3] Nanocomposites have gained prominence in pharmaceutical formulations and delivery applications due to their unique properties, including particulate size, surface characteristics, and antibacterial activities.[4,5] These composites combine the beneficial characteristics of both polymers and inorganic nanomaterials, resulting in unique functionalities suitable for medical applications. One of the primary advantages of polymeric/inorganic nanocomposites lies in their tunable properties. By varying the composition of the polymer matrix and the type and size of the inorganic nanoparticles, researchers can tailor the mechanical, thermal, and electrical properties of the resulting material to meet specific biomedical requirements. Further, the incorporation of inorganic nanoparticles can impart antimicrobial properties to the composite, making it effective against a wide range of

[a]*Polymers & Pigments Department, National Research Centre, Dokki, Giza 12622, Egypt. E-mail: ra.aly@nrc.sci.eg*
[b]*Chemistry Department, Faculty of Science, Capital University (formerly Helwan University), 11795 Helwan, Cairo, Egypt*

pathogens. This is particularly crucial in preventing infections associated with medical devices and implants. Moreover, these nanocomposites can enhance drug delivery systems. The incorporation of inorganic nanoparticles can facilitate the controlled release of therapeutic agents, allowing for localized treatment and reducing systemic side effects.[6,7]

The last few decades have seen a significant challenge in the synthesis of polymeric nanoparticles (PNPs), which can be produced either physically or chemically.[8] The main drawback of the physical method is that it frequently necessitates the use of either specialized equipment or a laborious procedure, raising the expense of producing these polymer nanoparticles, which frequently need to be protected. In the absence of this, the polymer particles will agglomerate and form blocks.[9]

The production of PNPs through the polymerization of monomers is described, focusing on primarily mini-, micro-, and emulsion polymerization approaches, whereas they are currently in use for the synthesis of a large number of environmentally friendly polymers with small nanoparticles.[10,11] Microemulsion polymerization is called low-energy emulsification method because it is a spontaneous-occurring process that does not need energy inputs. Microemulsions have unique qualities that make them suitable media for polymerization to produce nanoparticles thermodynamically stable, low viscosity, and are semi-transparency latex due to the uniformly dispersed tiny droplets.[12–14] A new sunscreen was successfully created by encapsulating zinc oxide nanoparticles (ZnO) and octocrylene in poly-styrene-*co*-methyl methacrylate (PMMA/PS) nanoparticles *via* minimemulsion polymerization. This new sunscreen has high encapsulation efficiency and favourable physical–chemical properties for use in sunscreens.[10]

Comparatively, due to its biocompatibility, poly(methyl methacrylate) (PMMA) is one of the biomedical materials that has been studied the most. There is increasing interest in its potential uses as a drug carrier, according to recent papers. Both pre-formed polymer-based processes and polymerization techniques can be used to create PMMA-based particulate carriers.[15,16] These particles have potential uses in medicine, such as serving as vaccine adjuvants and carriers of various medications, such as antioxidants and antibiotics, through various administration routes. Drugs are usually released from PMMA in a biphasic fashion with partial drug release. Recent approaches to improving release profiles have concentrated on making polymers more hydrophilic, such as by creating functionalized PMMA microspheres or combining hydrophilic polymers like HPMA and HEMA to form PMMA composites.[17–23]

Clindamycin hydrochloride (CDM) is a semi-synthetic analogue of the naturally occurring antibiotic lincomycin (7-chloro-7-deoxylincomycin hydrochloride). One of the most widely used antibacterial agents; it exhibits superior antimicrobial activity against both Gram-positive and Gram-negative bacteria. It is frequently applied topically to treat infections of the skin, soft tissues, and peritonitis, as well as acne. Certain methicillin-resistant *Staphylococcus aureus* infections may benefit from its use. Clindamycin is used to treat infections caused by numerous susceptible pathogenic aerobic bacteria in patients who are hypersensitive to penicillin.[24]

Clindamycin HCl was encapsulated inside various polymeric nanoparticles in previous articles (*e.g.* poly(lactic-*co*-glycolic acid), carboxymethyl chitosan, *etc.*) and suggested that the Cly loaded polymeric system improved the efficacy of clindamycin for the treatment of MRSA-infected wounds. Also, showed good antibacterial activity against *Staphylococcus aureus* and *C. acne*.[25,26]

The main objective of this work was, firstly, to prepare (ZnO NPs) using starch as a biopolymer stabilizer. Then using the prduced ZnO NPs to optimize the efficiency of clindamycin loaded polymeric system. Poly(MMA/HPMA) with different monomer ratios, poly(MMA/HPMA)/ZnO nanocomposites and that loaded with the medication clindamycin hydrochloride were created using an easy and low cost differential microemulsion copolymerization technique. The biocompatible co-emulsifier Tween-40 and Pluronic acid (F-68) was used to create nanoparticles (NPs) and stop coagulation. The MMA/HPMA composition, drug to copolymer ratio, and ZnO content of the suggested carriers have all been studied. Zeta potential, thermal stability, drug capture performance, *in vitro* drug release, and biological activity against two Gram-positive and Gram-negative bacteria have been investigated.

2 Experimental

2.1. Materials

Zinc sulfate heptahydrate ($ZnSO_4 \cdot 7H_2O$) and sodium hydroxide (NaOH) with purities of 99 and 97%, respectively, also, HCl and KCl were supplied from El-Nasr Pharmaceutical Chemicals Cairo Egypt. Starch with purity of 99% was obtained from Biotech Cairo Egypt. Monomers methyl methacrylate and hydroxypropyl-methacrylate (MMA and HPMA) were purchased from Sigma Aldrich Co. (Germany) and used after purification utilizing active Alumina columns. The purified MMA and HPMA were preserved in dark containers in a refrigerator for use within one month. Ammonium persulfate (APS; BDH laboratory Supplies Poole, BH15 1TD, England) was used as initiator. Tween40 (T-40; viscous liquid) and Pluronic-F-68 (powder) as non-ionic surfactants were purchased from Sigma-Aldrich (Germany). Clindamycin hydrochloride was provided as a gift from chemical industrial development CID Company. Potassium dihydrogen phosphate KH_2PO_4 was bought from Gen Lab (Egypt).

2.2. Synthesis of ZnO NPs

Zinc oxide nanoparticles (ZnO NPs) were created using a wet chemical precipitation process between $ZnSO_4 \cdot 7H_2O$ and NaOH in the presence of starch, a biopolymer stabilizing agent. A separate solution of $ZnSO_4 \cdot 7H_2O$, (0.1 M), NaOH (0.2 M), and starch (1%, w/v) was produced and vigorously stirred at 900 rpm. An aqueous stabilizer solution was then combined with the zinc salt solution, which was magnetically agitated at 750 rpm until a homogenous solution was achieved. The prepared NaOH solution was then added drop by drop to this combination solution, with continuous stirring then a white precipitate developed. The pH was continuously monitored

using a calibrated pH meter and maintained at 10 ± 0.2 using dropwise addition of NaOH while stirring. Following the completion of the reaction, the solution combination was kept overnight to age the precipitate. The recovered supernatant liquid was carefully cast off. Centrifugation (10 000 rpm for 10 min; Centurion Scientific Ltd, C2 series, West Sussex, UK) separated the settled white precipitate from the solution, which was then washed five times with deionized water DW using a sonicator (Qsonica, Newtown, USA) and centrifugation equipment. Washing was used to remove unreacted compounds, contaminants, and any ions or chemicals that the precipitate may have absorbed in order to reduce agglomeration. The precipitate was then dried in a laboratory oven at 80 °C overnight before being ground into fine powder. ZnO NPs were easily formed by calcining the dry powder at 400 °C for 2 hours in a muffle furnace (Thermolyne MF-8020, Gilson Co., Inc., Lewis Center, USA). The produced ZnO NPs are confirmed by UV-vis absorption peaks and characterized using FT-IR, zeta potential, and transmission electron microscopy (TEM).[27]

2.3. Synthesis of the polymeric nanospheres

With a monomer mixture MMA and HPMA (10% of all recipe), T-40 and P-F68 as co-emulsifiers, and APS as a water-soluble initiator, a differential microemulsion polymerization technique was used to create poly(MMA/HPMA) with varying monomer ratios as displayed in Scheme 1. A 250 mL three-necked round flask with a condenser and two dropping funnels was used to carry out the copolymerization reaction in a water bath with a temperature controller and mechanical stirring at 350 rpm.[28]

A mechanical stirrer was used to dissolve the T-40 and P-F-68 in 30 mL of deionized water (DW) in a flask. 3 mL of APS solution that has been prepared as 0.26 mmol in 15 mL DW, initially, was added to the emulsifier solution. Once the temperature reached the 65 °C decomposition temperature of the initiator, 10 mL of the APS solution and the required amount of monomers were gradually dropped to the aqueous phase *via* the dropping funnel over a period of approximately 0.5 hours accompanying with purging of a nitrogen.[29] The remaining 2 mL of the APS solution was added, and the solution was then allowed to polymerize for an additional two hours at 70 °C.[30] The polymeric nanosphere was produced in a homogeneous latex and semitransparent form.

2.4. Entrapment of the drug across microemulsion polymerization

The entrapment of the drug was occurred through *in situ* polymerization. Where, the predetermined amount of the water-soluble drug clindamycin hydrochloride was dissolved in the emulsifier aqueous solution in a monomer to drug ratio of 20 : 1 with different monomer feed composition and the effect of drug content was studied in two ratios of 20 : 1 and 10 : 1 at one monomer feed composition of MMA/HPMA$_{80/20}$. Then the differential micro-emulsion polymerization was carried out to form clindamycin hydrochloride-loaded polymeric.

2.5. Preparation of drug loaded poly(MMA/HPMA)/ZnO nanocomposites

Known weight ZnO NPs was suspended in the emulsifier solution aiding with a sonication apparatus for 10 min before being placed in the flask to form homogenous suspended nanoparticles with the procedure shown in Scheme 2. Then the *in situ* microemulsion polymerization was carried out as mentioned before to form a latex of poly(MMA/HPMA)/ZnO nanocomposites. ZnO NP was added in three percentages (1%, 3% and 5%) to the polymer composition of MMA/HPMA$_{80/20}$ with a monomer to drug ratio of 20 : 1.[15,18,31] The polymerization composition in every situation is illustrated in Table 1.

2.6. Characterization

Conversion and solid content measurements. Gravimetric measurements were made using a weighing method to ascertain the solid content of the generated nanolatex and the monomer conversion of the micro-emulsion polymerization.

Calculating the polymer latex's solid content (S%)

$$S\% = W_1/\ W_2 \times 100\%$$

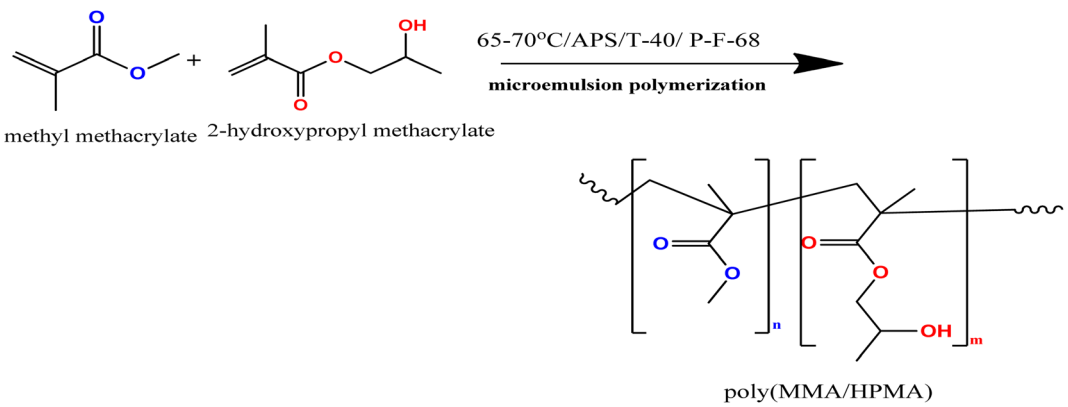

Scheme 1 Microemulsion polymerization of MMA and HPMA.

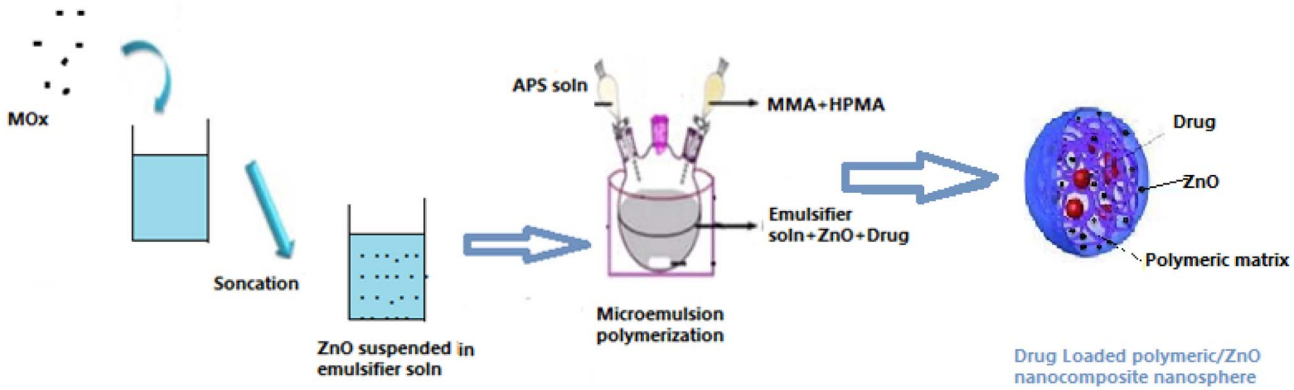

Scheme 2 Schematic representation for synthesis of clindamycin loaded-acrylate polymer/ZnO nanocomposite nanospheres.

Table 1 Polymerization composition

MMA	HPMA	Drug		ZnO		
100	0	20 : 1		—		
90	10	20 : 1		—		
20	20	20 : 1	10 : 1	—		
70	30	20 : 1		—		
80	20	20 : 1		1%	3%	5%

where W_1 is the weight of the dry polymer and W_2 is the weight of the polymer latex.

Monomer conversion percentage was calculated gravimetrically as follows:

$$\text{Conv.}\% = [P]/[M] \times 100$$

where $[P]$ is the dry polymer weight and $[M]$ is the inserted monomer mixture weight.

Morphology and particle size determination. Morphology and particle size of the polymeric nanospheres and nanocomposites were examined by Transmission Electron Microscope (TEM) using a JEOL JEM-2100 electronic microscope (JEOL, Ltd, Tokyo, Japan) with an accelerating voltage of 100 kV. Specimens for TEM measurements were prepared by depositing a droplet of polymer latex on a copper grid coated with carbon film (400 mesh), after which the solvent was evaporated in the air at 25 °C.

Entrapment efficiency of the drug. An ultracentrifuge was used to separate the poly(MMA/HPMA) nanospheres and the poly(MMA/HPMA)/ZnO nanocomposites loaded with the medication clindamycin hydrochloride from the aqueous latex while cooling at 50 000 rpm for 30 minutes. Using the indirect method, the drug's entrapment efficiency (EE) was calculated by measuring the amount of drug in the supernatant following the separation of the drug-loaded polymeric nanospheres. Using a standard calibration curve that was obtained experimentally by measuring the absorption of an aqueous solution of known drug concentrations ranging from 1 to 5 gm L^{-1}, the drug concentration was calculated by measuring the absorbance at λ_{max} 213 nm on a Shimadzu Ultraviolet–visible spectrophotometer. One can compute the drug's weight trapped in the polymeric nanospheres. The weight of the drug trapped in the polymeric nanoparticles divided by the weight of the drug that initially entered is known as the entrapment efficiency (EE%), and it may be expressed as follows using eqn (1):

$$\text{Entrapment efficiency } (\%) = \frac{(\text{the weight of the drug entrapped in the polymeric nanoparticles})}{\text{the weight of the drug initially used}} \times 100 \quad (1)$$

Zeta potential. The zeta potential of the nanospheres dispersed in a 1 mM solution of sodium chloride was determined by electrophoretic mobility at ambient temperature (25 °C) using the Zetasizer (Nano ZS, Malvern Instruments (3000-HS model) Ltd, UK).[31] The latex particles electrophoretic mobility (μ_e) was measured at various HPMA ratios. The zeta potential (ζ) was determined using the Smoluchowski's equation:

$$\zeta = \eta/\varepsilon \times \mu_e$$

where, (η) is the viscosity, and (ε) the permittivity of the medium.

FTIR spectroscopy. The IR spectrum of the free copolymer form and drug-loaded polymer was recorded on an IR spectrophotometer (PerkinElmer spectrophotometer) in the range of 400–4000 cm^{-1} using potassium bromide KBr pellets.

Thermal analysis. The thermal analysis was done by means of LINSEIS STA PT1600. A sample mass of about 3–5 mg was heated under nitrogen at the rate of 10 °C min^{-1} up to 1000 °C.

Change in weight, and the thermal behavior of the samples are recorded in the charts.[32]

X-ray diffraction analysis. Wide-angle goniometry and a diffractometer with a rotating target X-ray tube were used to identify X-ray diffraction patterns. A graphite monochromator with a voltage of 45 kV and a current of 40 mA was used to source the X-rays from a copper target. Over the course of two hours, the X-ray tube spanned scan intervals of 10° to 80° at a rate of 4° min^{-1} with 0.05° increments. XRD analysis was carried out for all samples (the drug, the polymer, drug loaded polymer, ZnO NPs and drug-loaded polymer/ZnO) to evaluate the effect of nanostructure implantation on the polymeric matrix of nanocomposites.[33]

***In vitro* drug release.** Clindamycin hydrochloride was tested for *in vitro* release from poly(MMA/HPMA) nanospheres and its nanocomposites with ZnO NPs using the dialysis bag technique in simulated intestinal and stomach fluid phosphate buffered saline media of pH 7.4 and 1.2, respectively.[18–21] The *in vitro* drug release experiments were triplicate and averaged. A buffer solution with a pH of 7.4 was made by mixing 250 mL of 0.1 M KH_2PO_4 and 195.5 mL of 0.1 M NaOH (to mimic intestinal fluid). A buffer solution with a pH of 1.2 (emulating stomach juice) was made by mixing 250 mL of 0.2 M HCl and 147 mL of 0.2 M KCl. Dialysis sacs were sink in the dissolution media a few hours to adjust to the dissolving liquid prior to studies. The dialysis bag (molecular weight cut-off 12 kDa, Sigma) was sink into the receptor compartment containing 50 mL of the dissolution media PBS and kept under stirring (100 rpm) at 37 ± 0.5 ° C. In 5 mL of buffer solution, 0.5 g of polymeric nanospheres or nanocomposites containing drugs were suspended.

The receptor compartment was sealed in order to prevent the evaporation of the dissolving media. Five millilitres of the sample were taken out for analysis every so often to check for released pharmaceuticals, and sink conditions were then maintained by introducing fresh buffer in an amount equal to that taken out. Samples were analyzed for drug content by using a calibration curve for clindamycin hydrochloride drug in each buffer solution by UV spectrophotometer at $\lambda_{max} = 204$ and 206 nm for pH 1.2 and 7.4, respectively.[19] The concentration of the released medication was then determined using the clindamycin hydrochloride standard curve, as shown in eqn (2), the percentage of drug released was determined from the following equation:

$$\text{Drug release (\%)} = \text{released drug/total loaded drug} \times 100. \quad (2)$$

Three separate release tests were conducted, and the results were averaged. The Korsmeyer–Peppas model was used to fit the release data in order to examine the drug release kinetics.[34]

Antibacterial activity. The antimicrobial activities of the poly(MMA/HPMA)/ZnO nanoscomposites were assessed and their effectiveness as antimicrobial agents were evaluated using the zone of inhibition method across the agar against different pathogenic microorganisms. This technique measures the effectiveness of a substance in preventing microbial growth on agar plates.[35]

In this method, a microbial strain is cultured on an agar plate, and the polymeric nanocomposite is dissolved in DMSO. The agar plate surface is inoculated by spreading a volume of the microbial inoculum over the entire agar surface. After incubation, which indicate the areas where microbial growth has been inhibited. The diameter of these zones is measured, providing a quantifiable measure of antimicrobial efficacy. This essay discusses the antimicrobial activity of the polymeric/ZnO nanocomposite, specifically focusing on its inhibitory effects against two Gram-positive bacteria, *Bacillus subtilis* and *Staphylococcus epidermidis*, as well as two Gram-negative bacteria, *Enterobacter cloacae* and *Escherichia coli*. The antimicrobial efficacy was determined through the measurement of the zone of inhibition (ZOI), which is the clear area surrounding the wells in which the polymer nanocomposite was placed.

2.7 Statistical analysis

Three separate experiments were carried out, and the results were presented as the mean ± standard deviation (SD). An analysis of ordinary two-way (ANOVA) with Tukey's multiple comparisons test was used to examine group differences for the swelling and release experiments. GraphPad Prism6 was used to determine the level of statistical significance. Results with a *p*-value of less than 0.05 were deemed to be substantially different.

3 Results and discussion

3.1. Synthesis of ZnO NPs using starch as a stabilizer

The optimum ZnO NPs sample synthesis was studied at various synthesis conditions and it was concluded that it was achieved using starch as biopolymer stabilizing agent with 1% (w/v) concentration, at room temperature (25 °C) for time as 0.5 hour, and with Zn salt to NaOH ratio as 1 : 2 $M_{Zn} : M_{NaOH}$ ratio. The optimum ZnO NPs synthesis was confirmed by UV-vis absorption peaks at λ_{max} as 346 nm when starch is added to zinc sulfate solution with 1% concentration.

Additionally, the appearance of particular bands corresponding to multiple functional groups in the FT-IR spectra (Fig. 1a) demonstrated that starch effectively functions as a capping agent for ZnO NPs. For instance, the distinctive bands that show the saccharide structure of starch include the O–H stretching broad band at 3290.20 cm^{-1}, the C–H stretching at 2930.11 cm^{-1}, the C–O–C stretching at 1148.05 cm^{-1}, and the C–O stretching at 1076.50 cm^{-1}. Additionally, the usual peaks that correspond to ZnO stretching vibrations show at 573.43 cm^{-1}, 522.51 cm^{-1}, and 438.15 cm^{-1}, confirming that ZnO NPs were successfully produced.[36] Functional groups on the surface of ZnO NPs can make these particles suitable for antibacterial and biomedical applications.

Furthermore, ZnO nanoparticles exhibit a zeta potential of −21.6 mV primarily due to the negative charge from surface hydroxylation in aqueous environments and the resulting electrostatic repulsion that stabilizes the nanoparticle suspension.

This zeta potential value suggests that the nanoparticles have a moderate negative charge, which can help keep them dispersed in a solution. This negative charge helps prevent the

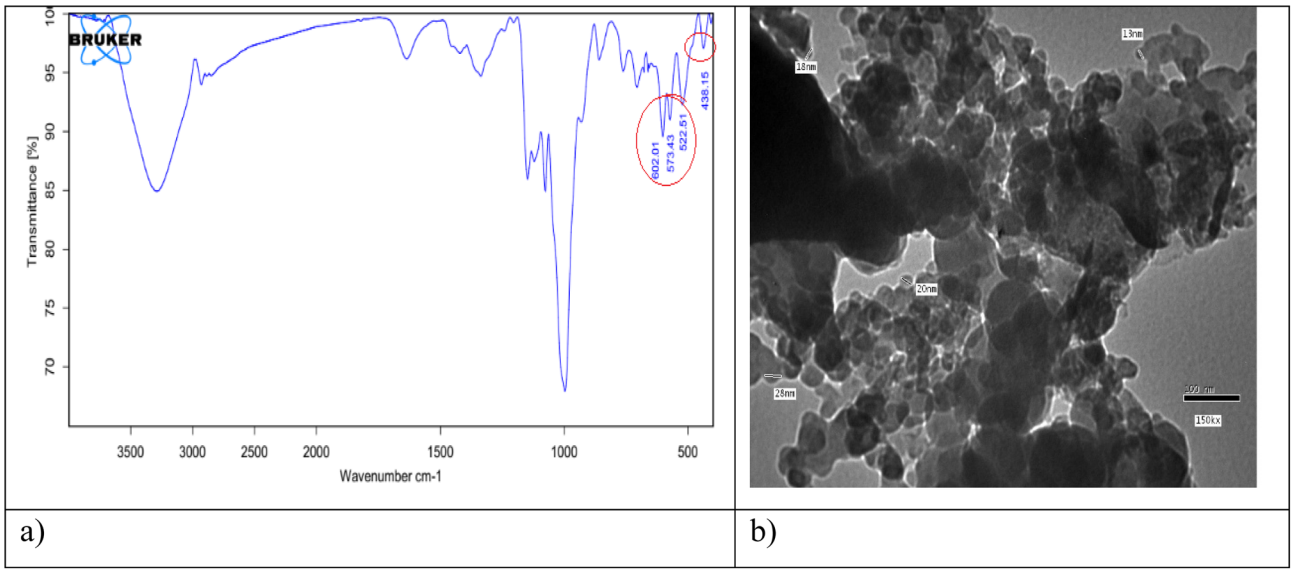

Fig. 1 (a) FT-IR spectra, and (b) TEM image of starch stabilized ZnO NPs.

particles from aggregating or clumping together, thus ensuring that the nanoparticles remain stable in suspension over time.

DLS analysis revealed a particle size range of 70 nm, however a TEM image (Fig. 1b) revealed that ZnO NPs were formed in the shape of almost spheres with an average particle size of 20 ± 2 nm. The particle size measured by DLS analysis is larger because it refers to the hydrodynamic size that involves not just the size of the particles themselves, but also the layer of solvent or medium that surrounds them. This "hydration shell" or "solvation shell" increases the effective size of the particles in a solution. Therefore, a more precise assessment of the actual particle size would be provided by methods such as transmission electron microscopy (TEM) or scanning electron microscopy (SEM).[37]

3.2. Preparation of the polymeric nanospheres

The free radical polymerization is a chain-growth process where a thermally decomposed initiator persulfate forming active free $^{\bullet}SO_4$ radicals that attack the monomer double bonds creating a new radical at the end of the monomer. This starts the polymer chain that keeps growing as long as there are available monomers, growing rapidly until termination.

With the least quantity of emulsifier, the differential microemulsion approach (in which the monomer mixture is added continuously) produced poly(MMA/HPMA) with nanospheres morphology that are nearly uniform in size and free of aggregates. This technique allowed an increase in HPMA content in the monomer feed composition of up to 40%. As well, the produced poly(MMA/HPMA) latex is thermodynamically stable and tolerant to additives such as inorganic and medicinal materials during *in situ* polymerization.[38] Well-defined polymeric nanospheres can be prepared with high conversion and high solid content as recorded in Table 2.

On the other hand, zeta potential measurements are obligatory to show the effect of HPMA and drug content on the charges of particles and the surface functionality effects on particle charge and stability. Zeta potential values showed that the sample with no HPMA exhibits slightly negative charges (−1.83 mV) that may be attributed to the negative charges of functionalities in the structure of the co-emulsifier system (Tween 40 and Pluronic- F-68). However, the negative charges become much higher in the presence of HPMA (−21.7 mV for MMA : HPMA ratio as 90 : 10), indicating a much higher degree of particle charging that can be attributed to the hydroxyl groups on the repeating units. But it is noted that further increasing of the HPMA content in the monomer feed composition in the samples led to a decrease in the negative charge that may be attributed to shielding by hydrocarbon chains (−8.11 mV for MMA : HPMA ratio as 70 : 30). By comparison between poly(MMA/HPMA)$_{80/20}$ and poly(MMA/HPMA)$_{80/20}$ loaded with the drug, it was noted that the zeta potential was affected slightly by clindamycin hydrochloride drug addition, whose values as −17.5, and −18.11 mV, respectively.

Table 2 The monomer conversion%, and zeta potential values for copolymerization of MMA and HPMA ratios as 100 : 0, 90 : 10, 80 : 20, and 70 : 30

Sample MMA : HPMA	Monomer conversion%	Zeta potential mV
100 : 0	95.5	−1.83
90 : 10	95.6	−21.7
80 : 20	100	−17.5
70 : 30	100	−8.11

3.3. Entrapment of the drug across microemulsion polymerization

Drug entrapment efficiency. The entrapment of clindamycin hydrochloride through differential micro-emulsion polymerization of MMA and HPMA in the presence of biocompatible co-

Table 3 Drug entrapment efficiency (EE)% presenting the effect of monomer feed composition, drug content and ZnO NPs content in the P(MMA/HPMA) nanospheres

A	Effect of monomer feed composition	MMA : HPMA	100 : 0	90 : 10	80 : 20	70 : 30
		EE%	62.480	63.149	62.22	62.14
		Solid content%	14.202	14.38	14.85	14.65
B	Effect of drug content	Drug : polymer ratio	1 : 20 (5%)	1 : 10 (10%)	—	—
		EE%	62.22	61.291		
		Solid content%				
C	Effect of ZnO NPs content	ZnO NPs%	0%	1%	3%	5%
		EE%	62.22	68.54	69.01	82.95
		Solid content%	14.85	14.91	15.1	15.43
		Conv.%	96.8%	96.5%	96%	95.8%

emulsifier T40/P-F68 was examined as a result of the variation of many factors, such as HPMA content in the monomer feed composition, the drug to monomer ratio (of 1 : 20 and 1 : 10) and the effect of zinc oxide nanoparticles ratio (ZnO NPs content).

The amount of drug loaded in nanospheres was measured indirectly by measuring the amount of unloaded drug dissolved in the supernatant using a UV-vis spectrophotometer at $\lambda_{max} =$ 213 nm for clindamycin hydrochloride in water solution using eqn (1). The drug EE% of the samples was determined and listed in Table 3. The entrapment efficiency (EE) was calculated. It is found that this system is excellent to incorporate clindamycin hydrochloride to give the value of entrapment efficiency (EE) of 65% and not cause agglomeration of the drug through polymerization.

It was observed that EE% values were not significantly changed with variations in HPMA and drug content, where they increased slightly in the first ratio.

On the contrary, the drug EE% values were extremely affected by ZnO NPs ratios of 1, 3, and 5%. As well, the drug is loaded with different amounts (with percentage of 5%, and 10% with respect to the monomer content). ZnO NPs caused increasing the entrapment efficiency so dramatically from ~62% to ~83% because it changes both the structure of the carrier system and the interactions with the drug. Where, the surface charges of ZnO NPs can result in stronger drug–carrier interactions through electrostatic interactions or coordination bonds. The very high surface area with porous or semi-porous structure due to the nano-sized particles that allows more drug molecules to adsorb onto or within the matrix. When ZnO is incorporated into systems like polymers, it can make the matrix more rigid and reduce leakage or diffusion of the drug during formation, so less drug is lost and higher entrapment efficiency.[39]

FTIR spectroscopy. The FTIR spectra for each of the MMA/HPMA copolymeric nanospheres with monomer feed

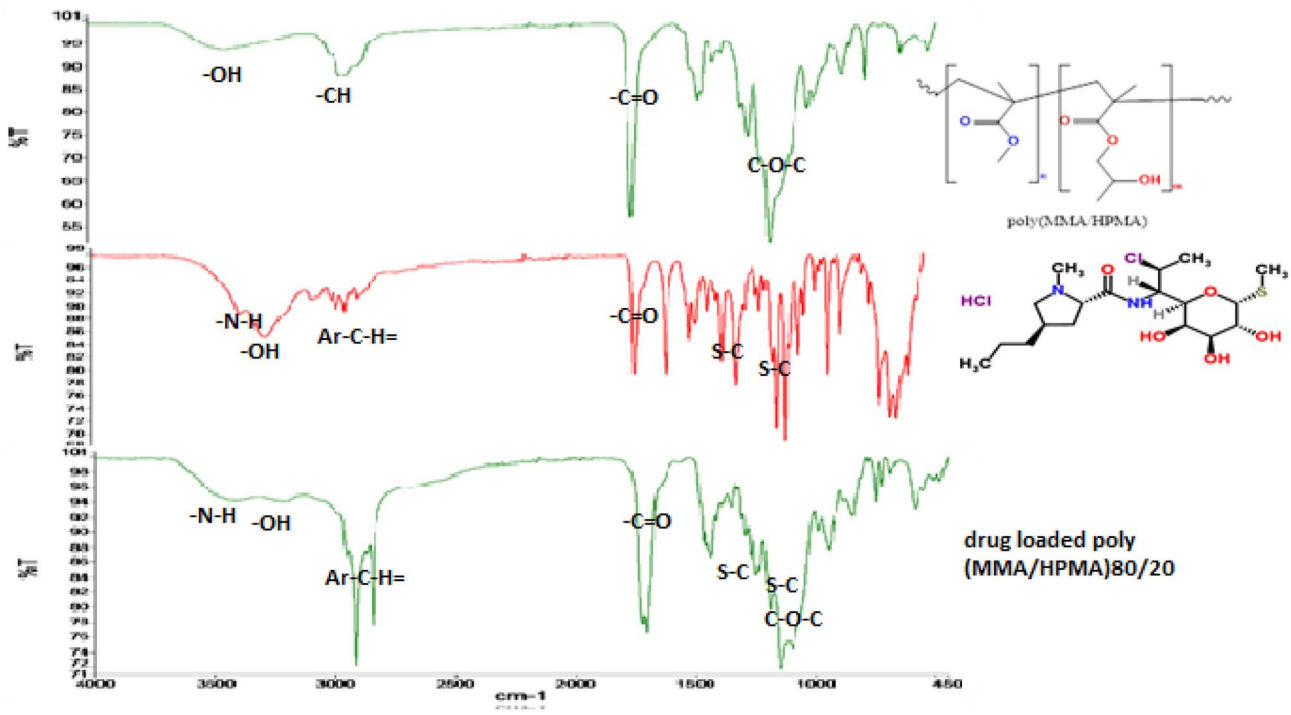

Fig. 2 FTIR spectra of poly(MMA/HPMA)$_{80/20}$, free clindamycin hydrochloride, and drug loaded-poly(MMA/HPMA)$_{80/20}$.

compositions of MMA/$HPMA_{80/20}$, free drug, and drug-loaded polymeric nanospheres (drug-loaded poly$(MMA/HPMA)_{80/20}$ are analyzed to confirm drug loading in these copolymers and are presented in Fig. (2). Where they show the details of the functional groups that characterize each fragment.

It was observed strong absorption at 3441.9 and 2949.90 cm^{-1} in the FTIR spectrum of poly$(MMA/HPMA)_{80/20}$ nanospheres, as shown in figure, corresponding O–H and C–H stretching vibrations, respectively. CH_3 and CH_2 deformations were responsible for multiple medium-to-strong bands in the 1724.80 to 1385.47 cm^{-1} region. The ester stretching vibration of the acrylate polymer, C–O–C asymmetric and symmetric vibrations are responsible for two strong bands at 1145.39 and 988.03 cm^{-1}, respectively. The C=O stretching vibration was identified as a sharp, intense band at 1724.80 cm^{-1}.

FT-IR spectra of clindamycin hydrochloride as free drug which provide information about the primary function groups found in the drug's structure. Strong absorption was seen at 3267.27 cm^{-1}, which is correlated with the N–H amide group, and 3062 cm^{-1}, which is correlated with the O–H stretching band. The aromatic C–H= stretch is represented by the bands at 3058.5 and 3025.7 cm^{-1} and the peaks of amide bond and S–C bond were observed at 1250 cm^{-1} and 1527 cm^{-1}. Furthermore, bands with a sharp intensity were discovered at 1682.93 cm^{-1}, which corresponds to the stretching vibration of C=O.[40,41]

FT-IR spectra of poly$(MMA/HPMA)_{80/20}$ loaded with clindamycin hydrochloride shows significant absorption at 2916.02 and a sharp, intense band was detected at 1720 cm^{-1}, corresponding to aliphatic C–H and carbonyl C=O stretches of the amido bond, respectively. Furthermore, strong absorption was observed above 2800 cm^{-1}, which are associated with the stretching vibrations of O–H and N–H, respectively. The ester stretching vibration of the acrylate polymer accounts for bands that appear at 1068 and 1261 cm^{-1}. The additional peaks of the amide bond and S–C bond were observed near 1250 cm^{-1} and 1530 cm^{-1}. Several medium-to-strong bands in the 1720.29 to 1271.46 cm^{-1} region were due to CH_3 and CH_2 deformations, and two strong bands at 1144.62 and 989.32 cm^{-1} are due to C–O–C asymmetric and symmetric vibrations, respectively.

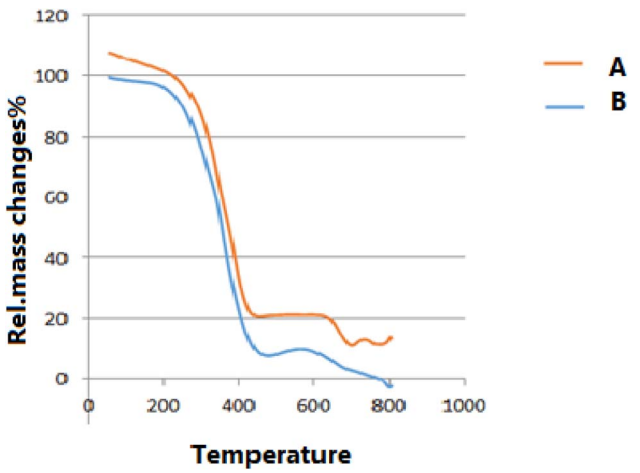

Fig. 3 TGA of (A) poly$(MMA/HPMA)_{80:20}$, (B) drug loaded-poly (MMA/$HPMA)_{80:20}$.

Table 4 Degradation temperatures and weight loss of (A) poly(MMA/$HPMA)_{80:20}$, (B) drug loaded-poly$(MMA/HPMA)_{80:20}$ and (C) drug loaded-poly$(MMA/HPMA)_{80:20}$/ZnO 5% nanocomposite

	Degradation temperatures		
Weight loss (%)	A	B	C
10	283.68	249.75	238
20	316.68	286.75	291.5
30	335.68	312.75	348
40	353.68	336.75	385.5
50	372.68	352.75	
60	388.63	367.75	
70	405.68	384.75	
80	477.68	405.75	
90	460.68	439.75	

Thermal gravimetric analysis (TGA). Free clindamycin hydrochloride suffer from thermal instability, so its entrapment into the acrylate polymer nanospheres can be referred by the increase of the thermal stability of the drug-loaded poly(MMA/$HPMA)_{80/20}$ compared with that of the free drug but less than

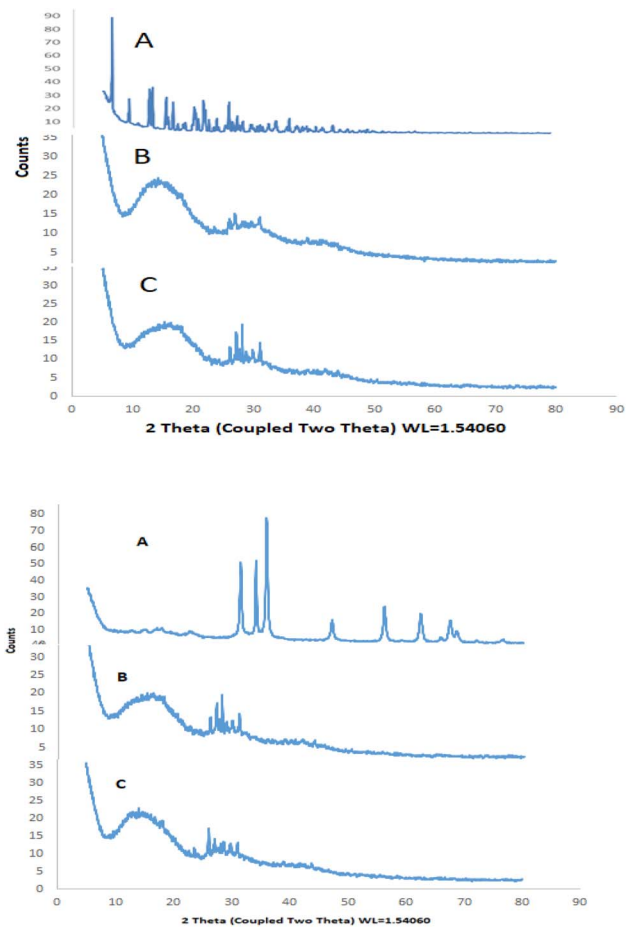

Fig. 4 : XRD of (I) (A) the free drug, (B) the free polymer, (C) the drug-loaded polymer, (II) (A) ZnO, (B) the drug-loaded polymer, and (C) the drug-loaded polymer/ZnO.

that of the free copolymer poly(MMA/HPMA)$_{80/20}$. The TGA results, which compare the temperatures at which the sample loses a certain percentage of its original weight, are displayed in Fig. 3 and values of these samples are shown in Table 4. *T*10% and *T*90% are the temperatures at which the samples lose 10% and 90% of their initial weights, respectively. It is noted that the entrapment of the drug inside poly(MMA/HPMA)$_{80/20}$ accept the drug high thermal stability, where the drug-loaded copolymer poly(MMA/HPMA)$_{80/20}$ lost only 20% of its initial weight at temperature 286.75 °C, so, it is characterized with high thermal stability but less than that of the free poly(MMA/HPMA)$_{80/20}$ that was considered as evidence to drug entrapment. Drug loading usually disrupts polymer structure, increases molecular mobility and lowers degradation temperature. In addition, drug incorporation can reduce polymer crystallinity that means less thermally stable.

Generally, it is appeared that this thermal decomposition occurred in two stages. The first stage occurred upto 316.68 °C for the free polymer and upto 286.75 °C for the drug-loaded polymer, through which the polymer lost only 20% of their initial weights. While the second stage is located between 316.6 °C and 405 °C and between 286.75 °C and 384 °C for the free polymer and the drug-loaded polymer, respectively, through which the polymer lost their weight faster 50% of their initial weights in narrow temperature raise range. In the next step, the weight lost is slow till temperature of 800 °C.

Additionally, the drug-loaded copolymer/ZnO nanocomposite exhibit high thermal stability with respect to the drug loaded copolymer and even the copolymer itself.[42,43] But the first 10% of its initial weight was lost at 238 °C that can be attributed to many factors. Early on, weak contacts, nucleation processes, or interface degradation may cause thermal stability to be lower than that of the pure polymer. But as the temperature rises later on, ZnO's stabilizing impact may become more noticeable. The strong thermal conductivity of zinc oxide may contribute to more uniform heat distribution throughout the composite material, improving thermal stability at higher temperatures.

It is clearly evident that the initial decomposition of the copolymer MMA/HPMA is much above the physiological temperature of 37 °C, and hence it is glassy in nature. Thus, they have a justly rigid chain structure, which gives significant

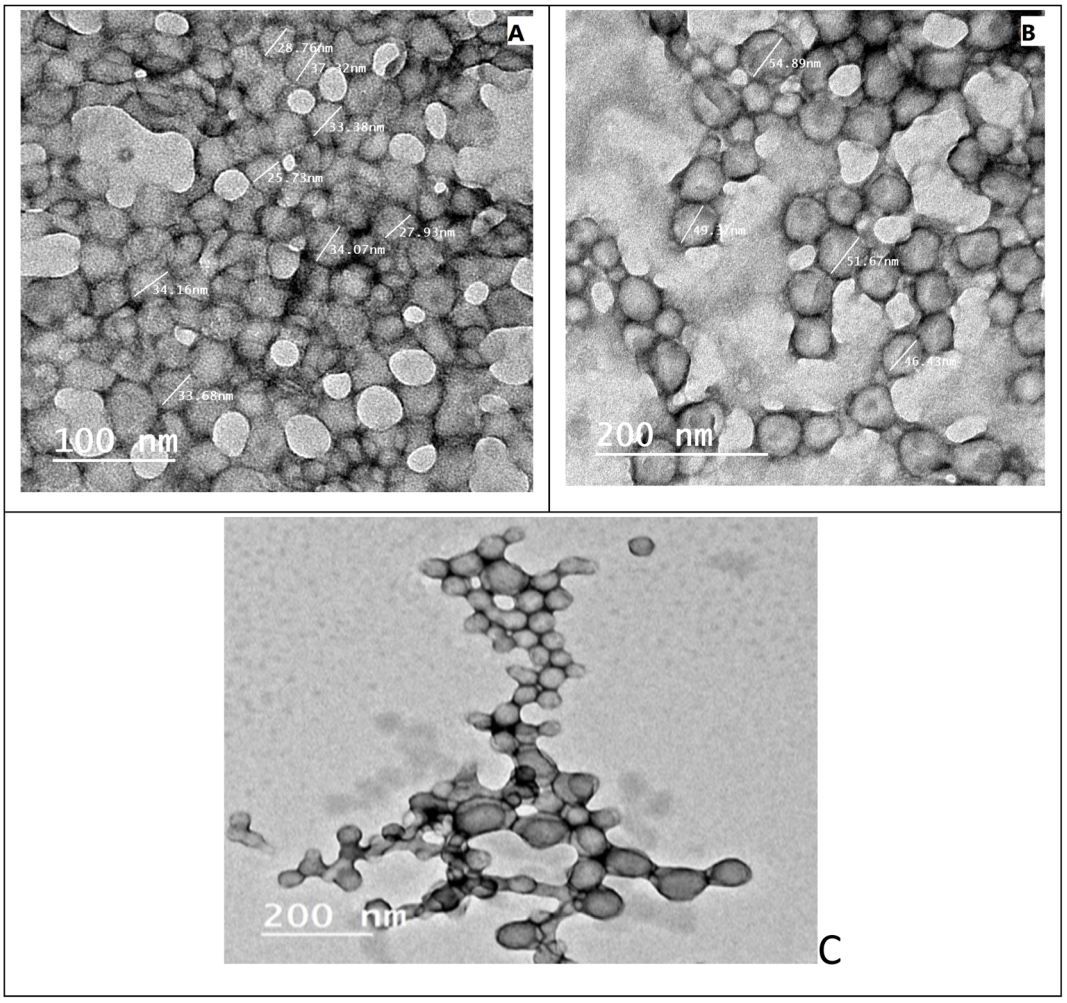

Fig. 5 TEM images of (A) poly(MMA/HPMA)$_{80/20}$, (B) drug loaded poly(MMA/HPMA)$_{80/20}$, and (C) drug loaded-poly(MMA/HPMA)$_{80:20}$/ZnO nanocomposite.

mechanical strength useful to drug delivery devices. So, the differential microemulsion polymerization of MMA and HPMA as a copolymer can be considered excellent for producing drug-loaded polymeric nanospheres in stable latex with a smaller size than 100 nm using a biocompatible emulsifier.

X-ray diffraction analysis. The structural characteristics of synthetic materials were investigated with the use of XRD. The XRD patterns for each free drug, free polymer, drug-loaded polymer, ZnO NP, and drug-loaded polymer-ZnO nanocomposite are shown in Fig. 5, to evaluate the effects of implanting nanostructures into the polymeric material matrix. It was clear from Fig. 5I that clindamycin hydrochloride is a polycrystalline substance with several distinctive peaks. Clindamycin hydrochloride's polycrystalline nature was indicated by many high-intensity peaks *e.g.*, at 2θ of 17.514, 20.166, 22.741, 26.112, 27.478, 28.417, 31.316, 34.195, 36.216, …; and peaks 6.496,9.367, 12.795, 13.237, 15.73, 16.74 showed the highest intensity.

As seen in Fig. 4, the pure polymer's XRD pattern shows peaks with a less intense shoulder at 2θ highest values of 12.730, 17.890 and 26.986 indicating a low crystalline structure system as reported in previous literature. The polymer's low degree of crystallinity indicates that it is mostly atactic.[44] Because the drug was distributed at the molecular level, the XRD patterns of the drug-loaded polymeric nanospheres and nanocomposites showed a drop in peak intensity when compared to the pure drug. The drug's entrapment within the polymer is indicated by the removal of some drug peaks and the decrease in intensity of others, which causes the encapsulated drug to transition to its disordered crystalline phase. Additionally, the distinct ZnO diffracted peaks situated at 2θ with highest values = 31.35, 33.99, 35.82, 47.06, 56.1, 62.31 and other peaks with less intensity. These XRD results revealed the crystalline nature with a hexagonal wurtzite structure for the ZnO nanoparticles.[45] By comparing with the drug-loaded polymer, the ZnO-based nanocomposite system exhibits similar behavior with a peak of comparable intensity and the ZnO characteristic peaks are reduced in the composite. It was observed that the addition of ZnO causes a shift in the peaks and can alter the polymer crystal planes. Where, the highest intense peak become at 2θ of 18.129 and 26.069 for the ZnO-based drug loaded nanocomposite, however, it was at 2θ of 27.174 and 28.144 for the drug-loaded polymeric nanospheres.

3.4 Morphological study and particle size

The size and morphologies of the polymeric nanospheres of poly(MMA/HPMA)$_{80:20}$ were displayed by TEM images. It was observed that the polymeric particles were narrowly distributed in size and had a distinctive spherical shape. TEM performance indicated that the microemulsion polymerization technique permits well entrapment of drugs while maintaining the spherical shape of nanoparticles, along with a slight increase in particle size after loading from an average of 30.5 nm to an average of 50.4 nm, based on comparison morphologies of the copolymer without and with drug loading and taking an average of 10 particle diameters. Furthermore, as Zhang *et al.* suggest, clindamycin entrapment can cause a significant morphological transformation.[46] This transformation indicates increased drug loading, and *vice versa*.

Fig. 5C shows TEM images of drug-loaded poly(MMA/HPMA)$_{80:20}$/ZnO nanocomposite with 3% ZnO NPs. This image indicates that the nanospheres have noticeable morphological changes that refer to the effective intercalation of both ZnO NPs and drugs with high loading of the drug within the polymeric nanospheres as spherical aggregates maintaining their diameter with an average of 50 nm. This is an indication of the binding of ZnO NPs to drug-loaded poly(MMA/HPMA)$_{80:20}$.

***In vitro* drug release studies.** A distinct weight of drug-loaded copolymeric nanospheres sample was suspended through dialysis bags in the dissolution media in closed container to maintain a sinking in constant volume throughout the release studies with a stirring rate of 100 rpm.

Two discrete physiological dissolution media were used: simulated intestinal fluid (pH 7.4) and gastric fluid (pH 1.2) at physiological temperature of 37 ± 0.5 °C. The concentration of the drug released in the dissolution media was measured by UV spectrophotometer at λ_{max} = 204 and 206 nm for pH 1.2 and 7.4, respectively, and the drug release % was calculated using eqn (2). The drug release behavior was studied as a function of a number of factors, such as the content of ZnO NPs, drug content, dissolution media, and monomer composition that are tested for their effects on drug release profiles.

The drug release profiles are plotted in (Fig. 6–8). Generally, it is noted that the drug released from the intended carriers typically shows an initial explosion effect in the first two hours, followed by a controlled release of the medication.

Effect of the monomer composition. Fig. 6 presents the different behaviour of the polymer with monomer composition ratios of MMA : HPMA as 90 : 10, 80 : 20, and 70 : 30 in both of the dissolution media at pH 7.4 and pH 1.2. The initial burst of drug was observed, followed by regular release, and it was noted that the existence of HPMA with a higher ratio triggered in a further enlargement in the rate of drug release depending on its ratio in both media. This behaviour of release can be attributed to the hydrophilicity of the polymer nanospheres caused by HPMA, which facilitates drug dissolution from the nanospheres.

Effect of the dissolution media and drug content. As well, drug release from the copolymeric nanospheres was influenced by the pH of the dissolution media, either simulated intestinal solution pH 7.4 or gastric solution pH 1.2. Where, no matter what the polymer composition was, the release rates reached maximum value in the intestinal fluid with pH 7.4. The drug release profiles are plotted in Fig. 7A and show that the release rates of clindamycin hydrochloride in the gastric fluid does not exceed 30% after 2 hours, while in the intestine fluid the amount of the released drug reached to 50% after 2 hours for the copolymer of (MMA/HPMA)$_{70:30}$.[14,15]

The drug release profiles that are plotted in Fig. 7B demonstrate that the drug content in the polymeric nanospheres has an effect on the quantity of the drug released, where the amount of the drug released from the copolymer loaded with a higher ratio of the drug (polymer : drug = 10 : 1) greater than that

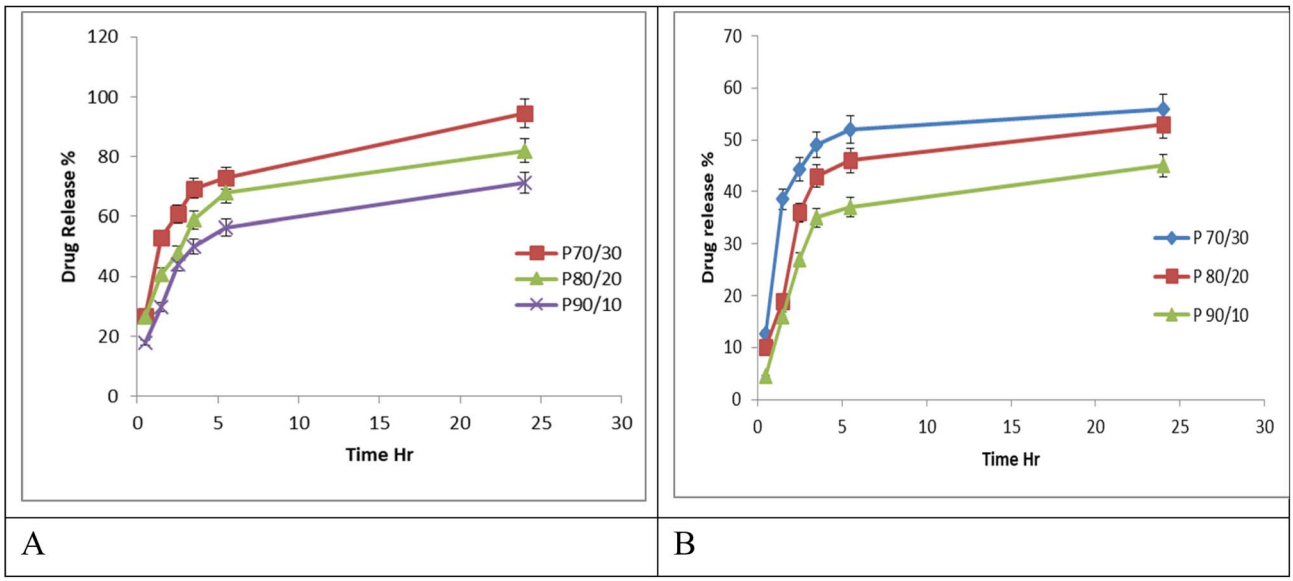

Fig. 6 *In vitro* drug release profiles from copolymer nanospheres of diverse MMA : HPMA ratios (90/10, 80/20, 70/30) in (A) simulated intestinal solution pH 7.4 and (B) simulated gastric solution pH 1.2. (Data are presented as mean ± S.D., $n = 3$). Where, $P < 0.0001$.

released from the copolymer loaded with a lower ratio of the drug (polymer : drug = 20 : 1).

Effect of ZnO NPS content. The rate of clindamycin hydrochloride release from the drug-loaded poly(MMA/HPMA)$_{90/10}$ nanospheres was compared with that containing 5% of ZnO NPs and is presented in Fig. 8. It was noted that ZnO NPs resulted in prolonged, controlled drug release profile. This behavior of release can be attributed to the fact that the presence of ZnO NPs may hinder drug dissolution from the nanospheres. Also, the release profile varied with the pH of the dissolution medium. The *in vitro* drug release studies revealed that incorporation of ZnO NPs in the copolymer nanospheres has not only improved the thermal stability of the nanocomposite but also exhibited more controlled and pH dependent release of clindamycin hydrochloride.[47]

It can be concluded that the *in vitro* drug release profiles from the clindamycin hydrochloride-loaded copolymeric nanospheres are dependent on many factors, such as the monomer composition, dissolution media, drug content, and ZnO NPs content in the polymeric nanospheres.

Antibacterial activity. The antibacterial activities of the tested sample either pristine polymer (sample no. 1), drug

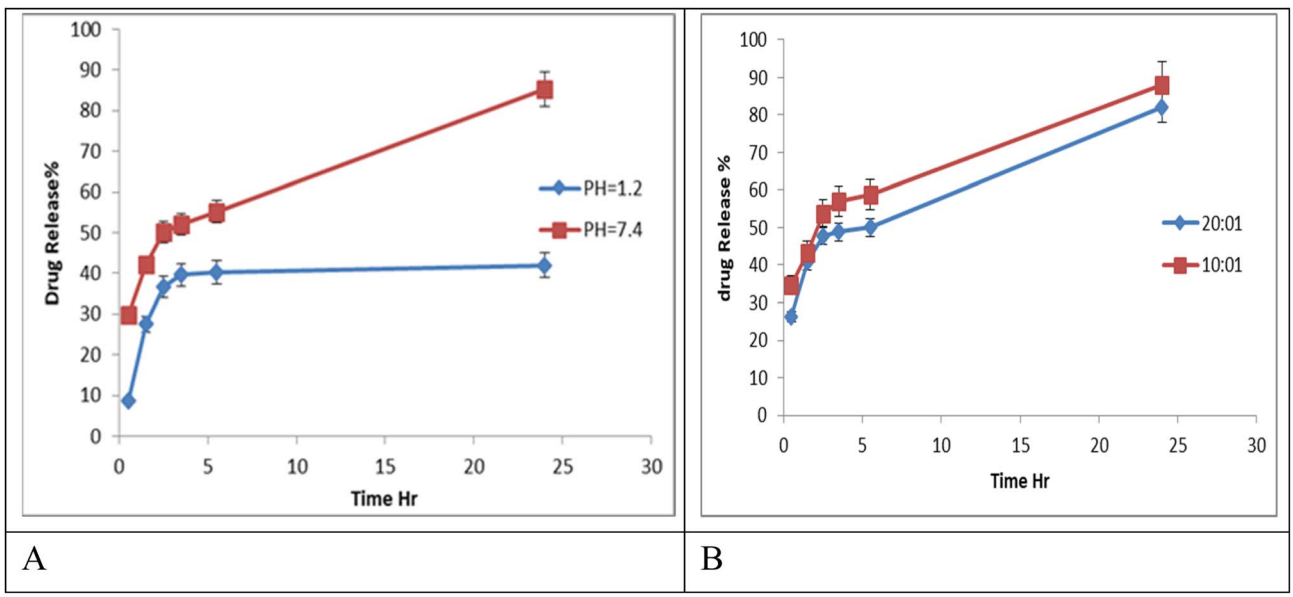

Fig. 7 *In vitro* drug release profiles from poly(MMA/HPMA)$_{90/10}$ nanospheres comparing the effect of pH of the dissolution media pH 7.4 and pH 1.2 (A) and the effect of polymer to drug ratio (20 : 1, 10 : 1) at pH 7.4 (B). (Data are presented as mean ± S.D., $n = 3$). Where, $P < 0.0001$.

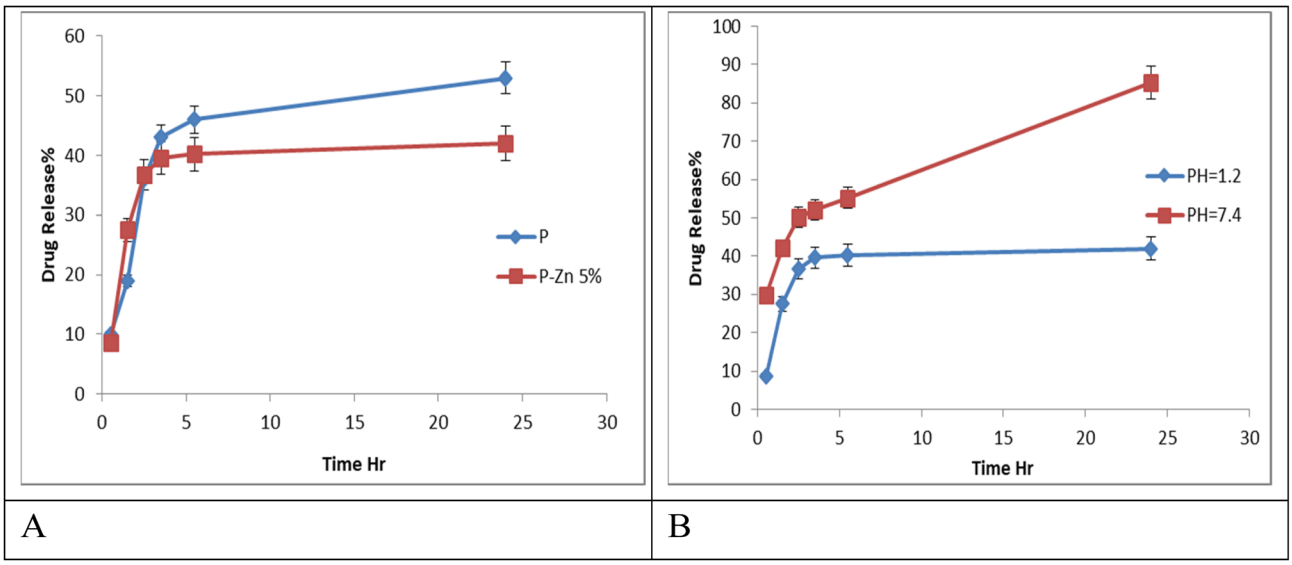

Fig. 8 Effect of ZnO NPs and the dissolution media on rate of drug release at pH = 1.2 and 7.4 from clindamycin hydrochloride-loaded copolymeric nanospheres with monomer feed composition of MMA : HPMA as 90/10. (Data are presented as mean ± S.D., $n = 3$). Where, $P < 0.0001$.

loaded polymer (sample no. 2), or drug loaded polymer/ZnO nanocomposite (sample no. 3) were evaluated against the different tested bacteria. Dimethyl sulfoxide, DMSO (D) was used as solvent and negative control. Reference drugs were used as positive control, Ciprofloxacin for Gram-positive and Gentamicin for Gram-negative strains with standard-sized (6 mm) filter paper discs impregnated with concentration of 10 micrograms. The well diffusion technique was applied due to its simplicity and cost-effectiveness. The antibacterial activity of polymer nanocomposite was evaluated based on the zone of inhibition (ZOI) against two Gram-positive bacteria, *Bacillus subtilis* and *Staphylococcus epidermidis*, as well as two Gram-negative bacteria, *Enterobacter cloacae* and *Escherichia coli*. The antibacterial activity of pure ZnO NPs was evaluated also in the current research.[9]

The clear ZOI created around the wells was detected and expressed in mm and their images are presented in Fig. (9). It was distinguished that poly(MMA/HPMA)/ZnO nanocomposites loaded with the clindamycin hydrochloride drug (sample no. 3) displays the highest antibacterial activities due to its unique characteristics. Where, the antibacterial effect of the nanocomposite is strengthened by many factors as nano-particles size and the antibacterial clindamycin hydrochloride drug.

Table 5 presents comparison in antibacterial activity of unloaded polymer, drug loaded polymer and drug loaded polymer/ZnO. It was observed that the highest ZOI for Gram-positive bacteria was 33 ± 0.82 mm and 34 ± 0.75 mm respectively in case of drug loaded polymer and polymer/ZnO nanocomposite with no activity (NA) in case of unloaded polymer in *B. subtilis*. For Gram-negative bacteria, the highest ZOI was 16 ±

Fig. 9 Antibacterial activity of polymer sample where, D: DMSO, sample no 1: the pristine polymer, sample no. 2: drug loaded polymer, and sample no. 3: the drug loaded polymer/ZnO nanocomposite.

Table 5 Mean zone of inhibition (ZOI) of the tested sample either ZnO NPs, pristine polymer, drug loaded polymer or drug loaded polymer/ZnO nanocomposite against the different tested bacteria

ZOI (mm)[a]					
Tested micro-organisms	ZnO NPs	P(MMA : HPMA)$_{80:20}$, (0% drug)	P(MMA : HPMA)$_{80:20}$ loaded (5% drug)	P(MMA : HPMA)$_{80:20}$, /ZnO 5%, drug 5%	Positive control[b]
Gram-positive bacteria					
B. subtilis	18 ± 0.12	NA	33 ± 0.82	34 ± 0.75	26 ± 0.21
S. epidermidis	14 ± 0.15	NA	NA	NA	24 ± 0.23
Gram-negative bacteria					
E. cloacae	16 ± 0.17	NA	16 ± 1.2	20 ± 0.6	30 ± 0.25
E. coli	10 ± 0.19	NA	NA	NA	30 ± 0.24

[a] Results are expressed as the mean of three separate trials ± standard deviation. [b] Reference drugs: ciprofloxacin for Gram-positive and gentamicin for Gram-negative strains.

1.2 mm and 20 ± 0.6 mm respectively in case of drug loaded polymer and drug loaded polymer/ZnO nanocomposite with no activity in case of unloaded polymer in *E. cloacae* whereas *E. coli* showed no antibacterial activity. We can conclude that, the highest inhibitory action of the tested polymers and nanocomposite was manifested against *B. subtilis* followed by *E. cloacae*. Besides, polymer/ZnO nanocomposite showed a higher antibacterial effect against Gram-positive than the Gram-negative bacteria. It was shown that Gram-negative bacteria are typically more resistant because they have a double membrane, with an outer membrane that acts as a strong barrier to many substances, including antibiotics. This membrane contains lipopolysaccharides (LPS), which make it harder for certain drugs to penetrate the cell.

In contrast, Gram-positive bacteria have a thicker peptidoglycan layer but lack the outer membrane, so antibiotics can more easily pass through the cell wall to reach the inner membrane. Also, the negatively charged surfaces, which were approved from zeta potential measurements, repel negatively charged bacterial cells due to electrostatic interactions, which is a fundamental aspect of their antibacterial activity. Most bacterial cell membranes carry a net negative charge. When these bacteria approach a negatively charged surface, the repulsive force inhibits their growth. Different techniques are used to evaluate antibacterial activity *in vitro*. The most common one is through the agar.[48,49]

Some possible antibacterial mechanisms were proposed in the literature to understand the antibacterial activity of ZnO NPs.[50]

(a) ZnO NPs gradually release Zn^{2+} ions in this mechanism, which can enter the cell membrane and cause denaturation of proteins and the stoppage of cell division. In addition, cellular respiratory disorders can be brought on by Zn^{2+}-induced damage to the electron transport system. ZnO NPs release toxic Zn^{2+} ions that inhibit a variety of bacterial cell functions, including enzyme activity and metabolism, ultimately leading to bacterial cell death.[51]

(b) Production of reactive oxygen species (ROS): one of the well-known mechanisms for ZnO NPs' ability to inhibit bacterial growth is the ROS that are produced from their surface. The

Table 6 Comparison of the present clindamycin nanocarrier with the previously reported

Composites	Antibiotic	Particle size (nm)	Release	EE%	Drug loading	Ref.
PLGA-based nanocomposite and chitosan/bioglass system	Cly+ (ciprofloxacin [CIP], metronidazole [MET]	From 199.6 ± 41.5 to 305.2 ± 70	Fast	60 ± 0.10	10 ± 0.02%	55
Polyhydroxyalkanoates (Cly-PHA NPs)	Cly	(216.2 ± 38)	Sustained		(6.76 ± 0.19%)	56
ZnO NPs	Cly	200 ± 10 to 169.7 ± 9	Sustained, controlled and prolonged	83 ± 0.4	From 5% to 20%	57
ZnO NPs that was synthesized by green precipitation	Cly	44.63				58
Poly(lactic-*co*-glycolic acid)-polyethylenimine (PLGA-PEI)NPs and (PLGA)NPs	Cly	126 ± 33 and 132 ± 41	Sustained drug release		1.31 ± 0.3 and 1.43 ± 0.5	25
PMMA/(PLGA)	Cly					59
Carbopol/ZnO NPs gel	—	From 9 to ∼93				60
P(MMA/HPMA)/ZnO NPs	Cly	From 31.78 to 50	Sustained drug release	82.95%	From 5% to 10%	This work

reactive oxygen species (ROS) that cause lethal damage to bacteria include superoxide anion (O_2^-), hydroxyl radical ($^{\bullet}OH$), peroxide anion (O_2^{2-}) hydroxyl anion (OH^-), and hydrogen peroxide (H_2O_2) species. Because ROS produce oxidative stress, damage to DNA, cell membranes, and cellular proteins can be observed. The production of ROS also results in cell death because it destroys the active components that keep the microorganism functioning normally in terms of morphology and physiology.[52,53]

(c) ZnO NPs directly interacting with cell membrane: whereby ZnO NPs directly interact with the bacterial cell membrane through electrostatic forces, causing microenvironmental changes in the bacterial cell and NP contact areas. This interaction may change the structure of the membrane, allowing intracellular material to leak out and ultimately leading to cell death.[54]

The current drug nano-carrier system [cly-loaded poly(MMA/HPMA)/ZnO NPs] offers many advantages, including ease of preparation, low cost, nano-sized particles (up to 50 nm) with excellent drug loading and entrapment efficiency%, as well as being a very good growing inhibitor for *B. subtilis* bacteria. This is evident when we compare the current work with the previously reported antibacterial effects *via* clindamycin with or without ZnO NPs, as shown in Table 6.

4 Conclusion

In this study, ZnO NPs were successfully synthesized with an average particle size as 20 nm providing high yield using starch as biopolymer stabilizing agent with 1% (w/v) concentration, at room temperature (25 °C) for time as 0.5 hour, and with Zn salt to NaOH ratio as 1 : 2. Furthermore, well controlled sustained, prolonged, and pH-sensitive drug delivery system composed of methyl methacrylate/hydroxypropyl methacrylate (MMA/HPMA) copolymer incorporated with ZnO NPs in various contents were successfully synthesized using an *in situ* microemulsion polymerization technique. This acrylate polymer/ZnO NPs nanocomposite showed high efficiency to entrapment of clindamycin hydrochloride as an effective thermally stable smart drug delivery system that was described through TGA, TEM, FTIR, and zeta potential. Entirely magnitudes demonstrated that the morphological and structural characteristics, entrapment efficiency (EE%), and *in vitro* drug release were influenced by the MMA/HPMA ratio and contents of the drug and ZnO NPs.

Besides, it was noticeable that the embedding of ZnO NPs in the polymeric nanocomposite elevated the high EE% value (82.95%) compared with 62.22% in absence of ZnO NPs, allowing for the loading of a larger amount of drug and, likewise, amplified the prolongation and control of the drug release.

Moreover, the drug-loaded polymer/ZnO nanocomposite showed a significant antibacterial effect against both *B. subtilis* and *E. cloacae*, but this effectiveness against Gram-positive was more than the Gram-negative bacteria.

Conflicts of interest

We have no conflicts of interest.

Data availability

Data available on request from the authors.

References

1 G. Abdel-Maksoud, R. A. Sobh and A. Tarek, Evaluation of MMI/acrylate nanocomposite with hydroxyapatite as a novel paste for gap filling of archaeological bones, *J. Cult. Herit.*, 2022, **57**, 194–204, DOI: 10.1016/j.culher.2022.08.013.
2 W. S. Mohamed, R. A. Sobh, H. E. Nasr and A. M. Eid, Study the Ultrasonic Assisted for Polymeric Nanocomposite, *Egypt. J. Chem.*, 2017, **60**, 109–128, DOI: 10.21608/ejchem.2017.686.1017.
3 S. S. Darwish, R. A. Sobh, N. H. Atiya and D. Y. Mahmoud, Evaluation of the effectiveness of some volatile oils and chemical insecticides were added to Silver Nanoparticles used for the treatment of infected dyed woolen textile with museum insect pests *Anthrenus verbasci*, *Egypt. J. Chem.*, 2022, **65**(2), 509–519, DOI: 10.21608/ejchem.2021.89087.4279.
4 S. A. Abou Taleb, R. A. Sobh and R. M. Mourad, Investigating the Effect of Loading Curcuminoids Using PCL-PU-βCD Nano- Composites on Physico-Chemical Properties, *In Vitro* Release, and *Ex Vivo* Breast Cancer Cell-Line, *Biointerface Res. Appl. Chem.*, 2022, **12**(3), 4074–4102, DOI: 10.33263/briac123.40744102.
5 W. S. Mohamed, H. E. Nasr, R. Gutmann and R. A. Sobh, Effect of CaO nanoparticles on the properties of polyamide 6, *Egypt. J. Chem.*, 2015, **58**(3), 365–375.
6 R. A. Sobh, B. Ekram and W. S. Mohamed, Fabrication of acrylic modified surface of polyamide 6/CaO electrospun nanofibrous membrane for effective dye removal, *Egypt. J. Chem.*, 2020, **63**(6), 2249–2260, DOI: 10.21608/ejchem.2019.19498.2187.
7 A. Ghazzy, R. R. Naik and A. K. Shakya, Metal–Polymer Nanocomposites: A Promising Approach to Antibacterial Materials, *Polymers*, 2023, **15**, 2167, DOI: 10.3390/polym15092167.
8 H. B. Mohamed, R. A. Sobh, N. El-Hadidi and S. S. Darwish, A Comparative Study to Evaluate Regalrez, Nano Regalrez, and Nano Composite for the Consolidation of Pigments used on Ancient Egyptian Wooden Artifacts, *Egypt. J. Chem.*, 2025, **68**(2), 47–61, DOI: 10.21608/ejchem.2024.286559.9670.
9 N. Al-Harbi and N. K. Abd-Elrahman, Physical methods for preparation of nanomaterials, their characterization and applications: a review, *Journal of Umm Al-Qura University for Applied Sciences*, 2025, **11**, 356–377, DOI: 10.1007/s43994-024-00165-7.
10 P. P. Pandey, Preparation and Characterization of Polymer Nanocomposites, *Soft Nanosci. Lett.*, 2020, **10**, 1–15, DOI: 10.4236/snl.2020.101001.
11 M. S. Frizzo, P. E. Feuser, P. H. Berres, E. Ricci-Junior, C. E. M. Campops, C. Costa, P. H. H. de Araujo and C. Sayer, Simultaneous encapsulation of zinc oxide and octocrylene in poly(methyl methacrylate–styrene) nanoparticles obtained by miniemulsion polymerization

for use in sunscreen formulations, *Colloids Surf., A*, 2019, **561**, 39–46, DOI: 10.1016/j.colsurfa.2018.10.062.

12 R. A. Sobh, H. E. Nasr and W. S. Mohamed, Synthesis and characterization of magnetic sponge nanocomposite for cleaning archeological lime stone, *Egypt. J. Chem.*, 2020, **63**(2), 507–514, DOI: 10.21608/ejchem.2019.18448.2141.

13 G. Abdel-Maksoud, R. A. Sobh, A. Tarek and S. H. Samaha, Evaluation of Montmorillonite (MMT)/polymer nanocomposite in gap filling of archaeological bones, *Egypt. J. Chem.*, 2020, **3**(5), 1585–1603, DOI: 10.21608/ejchem.2019.15761.205.

14 R. A. Sobh, H. E. Nasr and W. S. Mohamed, Formulation and *in vitro* characterization of anticancer drugs encapsulated Chitosan/Multi-walled carbon nanotube nanocomposites, *J. Appl. Pharm. Sci.*, 2019, **9**(08), 32–40, DOI: 10.7324/JAPS.2019.90805.

15 R. A. Sobh, H. E. Nasr, A. B. Moustafa and W. S. Mohamed, Tailoring of anticancer drugs loaded in MWCNT/poly(MMA-*co*-HEMA) nanosphere composite by using *in situ* microemulsion polymerization, *J. Pharm. Invest.*, 2019, **49**, 45–55, DOI: 10.1007/s40005-018-0390-8.

16 M. N. A. Said, N. A. Hasbullah, M. R. H. Rosdi, M. S. Musa, A. Rusli, A. Ariffin and M. D. Shafiq, Polymerization and Applications of Poly(methyl methacrylate)–Graphene Oxide Nanocomposites: A Review, *ACS Omega*, 2022, **7**, 47490–47503, DOI: 10.1021/acsomega.2c04483.

17 P. E. Feuser, L. S. Bubniak, M. C. S. Silva, A. C. Viegas, A. C. Fernandes, *et al*, Encapsulation of magnetic nanoparticles in poly(methyl methacrylate) by miniemulsion and evaluation of hyperthermia in U87MG cells, *Eur. Polym. J.*, 2015, **68**, 355–365, DOI: 10.1016/j.eurpolymj.2015.04.029.

18 M. K. Darwish, M. Shaban, R. A. Sobh and A. A. A. Khalek, Tailoring nano copolymer/CNTs composite and its application in drug delivery, *Egypt. J. Chem.*, 2021, **64**(7), 3335–3349, DOI: 10.21608/ejchem.2021.60541.3303.

19 R. A. Sobh, W. S. Mohamed, A. B. Moustafa and H. E. Nasr, Encapsulation of Curcumin and Curcumin derivative in polymeric nanospheres, *Polym.-Plast. Technol. Eng.*, 2015, **54**, 1457–1467, DOI: 10.1080/03602559.2014.1003230.

20 A. B. Moustafa, R. A. Sobh, A. M. Rabie, H. E. Nasr and M. M. H. Ayoub, Synthesis and *in vitro* release of guest drugs-loaded copolymer nanospheres MMA/HEMA *via* differential microemulsion polymerization, *J. Appl. Polym. Sci.*, 2013, **129**(2), 853–865, DOI: 10.1002/app.38635.

21 A. B. Moustafa, R. A. Sobh, A. M. Rabie, H. E. Nasr and M. M. H. Ayoub, Differential microemulsion polymerization as a new root for entrapment of drugs, *J. Appl. Polym. Sci.*, 2013, **127**(6), 4634–4643, DOI: 10.1002/app.38059.

22 A. Bettencourt and A. J. Almeida, Poly(methyl methacrylate) particulate carriers in drug delivery, *J. Microencapsul.*, 2012, **29**(4), 353–367, DOI: 10.3109/02652048.2011.651500.

23 J. Kreuter, Poly(Methyl Methacrylate) Nanoparticles As Vaccine Adjuvants, in *Book: Vaccine Adjuvants*, 2008, pp. 105–119, DOI: 10.1385/1-59259-083-7:105.

24 K. Pauter, M. Szultka-Młyńska and B. Buszewski, Determination and Identification of Antibiotic Drugs and Bacterial Strains in Biological Samples, *Molecules*, 2020, **25**(11), 2556, DOI: 10.3390/molecules25112556.

25 N. Hasan, J. Cao, J. Lee, S. P. Hlaing, M. A. Oshi, M. Naeem, *et al.*, Bacteria-Targeted Clindamycin Loaded Polymeric Nanoparticles: Effect of Surface Charge on Nanoparticle Adhesion to MRSA, Antibacterial Activity, and Wound Healing, *Pharmaceutics*, 2019, **11**, 236, DOI: 10.3390/pharmaceutics11050236.

26 T. Chaiwarit, S. R. Sommano, P. Rachtanapun, N. Kantrong, W. Ruksiriwanich, M. Kumpugdee-Vollrath and P. Jantrawut, Development of Carboxymethyl Chitosan Nanoparticles Prepared by Ultrasound-Assisted Technique for a Clindamycin HCl Carrier, *Polymers*, 2022, **14**, 1–20, DOI: 10.3390/polym14091736.

27 T. F. Hassanein, A. S. Mohammed, W. S. Mohamed, R. A. Sobh and M. K. Zahran, Optimized synthesis of biopolymer-based zinc oxide nanoparticles and evaluation of their antibacterial activity, *Egypt. J. Chem.*, 2021, **64**(7), 3767–3790, DOI: 10.21608/ejchem.2021.75677.3709.

28 R. A. Sobh, H. S. Magar, H. A. Abd El Salam and H. E. Nasr, Acrylate polymeric nanocomposites embedded with transition metal triazole complexes: synthesis, characterization, and prospective implement as hydrogen peroxide sensors, *J. Nanopart. Res.*, 2024, **26**(8), 197, DOI: 10.1007/s11051-024-06075-3.

29 A. N. Shehab-ElDin, R. A. Sobh, A. M. Rabie, W. S. Mohamed and H. E. Nasr, Polyacrylamide Grafted Electrospun Polyamide 6 Nanocomposite Fibers for Drug Delivery Application, *Egypt. J. Chem.*, 2022, **65**(5), 33–47, DOI: 10.21608/ejchem.2022.119754.5386.

30 H. S. Magar, M. S. Hashem and R. A. Sobh, Design of metal oxide nanoparticles-embedded polymeric nanocomposites for hydrogen peroxide chronoamperometric sensor, December 2023, *Polym. Compos.*, 2024, **45**, 3653–3665, DOI: 10.1002/pc.28017.

31 R. A. Sobh, H. S. Magar, A. M. Fahim and M. S. Hashem, Construction, molecular docking simulation and evaluation of electrochemical properties of polymeric nanospheres comprising novel synthesized monomer *via* green microemulsion polymerization, *Polym. Adv. Technol.*, 2023, **35**(1), e6248, DOI: 10.1002/pat.6248.

32 J. A. C. Barbosa, M. S. E. Abdelsadig, B. R. Conway and H. A. Merchant, Using zeta potential to study the ionisation behaviour of polymers employed in modified-release dosage forms and estimating their pKa, *Internet J. Pharmacol.*, 2019, **1**, 100024, DOI: 10.1016/j.ijpx.2019.100024.

33 R. A. Sobh, H. S. Magar, A. M. Fahim, H. M. El-Masry and M. S. Hashem, Fabrication and Evaluation of Polyacrylate Nanocomposites Embedded With Metal Oxides as Enhanced Multipurpose Nanocarriers for Long-Term Anti-Inflammatory and Amazing Antimicrobial Properties, *Appl. Organomet. Chem.*, 2025, **39**(1–19), e7862.

34 A. N. Shehab-ElDin, R. A. Sobh, A. M. Rabie, W. S. Mohamed and H. E. Nasr, Polyamide 6/tallow modified clay

nanofibrous mat coupled with hydrogels for potential topical/transdermal delivery of doxycycline hydrochloride, *J. Pharm. Invest.*, 2023, **53**, 307–321.

35 T. J. Hossain, Methods for screening and evaluation of antimicrobial activity: a review of protocols, advantages, and limitations, *Eur. J. Microbiol. Immunol.*, 2024, **14**(2), 97–115, DOI: 10.1556/1886.2024.00035.

36 E. Darvishi, D. Kahrizi and E. Arkan, Comparison of different properties of zinc oxide nanoparticles synthesized by the green (using *Juglans regia* L. leaf extract) and chemical methods, *J. Mol. Liq.*, 2019, **286**, 110831, DOI: 10.1016/j.molliq.2019.04.108.

37 S. Filippov, R. Khusnutdinov, A. Murmiliuk, *et al*, Dynamic light scattering and transmission electron microscopy in drug delivery: a roadmap for correct characterization of nanoparticles and interpretation of results, *Mater. Horiz.*, 2023, **10**(12), 5354–5370, DOI: 10.1039/D3MH00717K.

38 R. A. Sobh and H. S. Magar, Innovative formulation of a functional nano-copolymer derived from glycidyl methacrylate and acrylonitrile as an exceptionally sensitive and selective electrochemical sensor for folic acid detection in pharmaceutical and food samples, *Nanoscale*, 2025, **17**, 18359–18376.

39 S. Islam, M. M. S. Ahmed, M. A. Islam, N. Hossain and M. A. Chowdhury, Advances in nanoparticles in targeted drug delivery–a review, *Results Surf. Interfaces*, 2025, **19**, 100529, DOI: 10.1016/j.rsurfi.2025.100529.

40 X. Zhu, M. Su, S. Tang, L. Wang, X. Liang, F. Meng, Y. Hong and Z. Xu, Synthesis of thiolated chitosan and preparation nanoparticles with sodium alginate for ocular drug delivery, *Mol. Vision*, 2012, **18**, 1973–1982. https://www.molvis.org/molvis/v18/a207.

41 E. Dinte, E. Bodoki, S. Leucuta and C. A. Iuga, Compatibility studies between drugs and excipients in the preformulation phase of Buccal Mucoadhesive systems, *Farmacia*, 2013, **61**(4), 703–712. https://www.researchgate.net/publication/256094226.

42 S. Thipperudrappa, A. U. Kini and A. Hiremath, Influence of zinc oxide nanoparticles on the mechanical and thermal responses of glass fiber-reinforced epoxy nanocomposites, *Polym. Compos.*, 2020, **41**, 174–181, DOI: 10.1002/pc.25357.

43 A. H. Farha, A. F. Al Naim and S. A. Mansour, Thermal Degradation of Polystyrene (PS) Nanocomposites Loaded with Sol Gel-Synthesized ZnO Nanorods, *Polymers*, 2020, **12**, 1935, DOI: 10.3390/polym12091935.

44 R. C. de Azevedo Gonçalves Mota, E. O. da Silva and L. R. de Menezes, Effect of the addiction of metal oxide nanoparticles on the physical, chemical and thermal properties of PVA based nano-composites, *Mater. Sci. Appl.*, 2018, **9**, 473–488, DOI: 10.4236/msa.2018.95033.

45 M. R. Arefi and S. Rezaei-Zarchi, Synthesis of Zinc Oxide Nanoparticles and Their Effect on the Compressive Strength and Setting Time of Self-Compacted Concrete Paste as Cementitious Composites, *Int. J. Mol. Sci.*, 2012, **13**, 4340–4350, DOI: 10.3390/ijms13044340.

46 L. Zhang, X. Li, Z. Wang, S. Wu and J. Ma, Cellulose controlled zinc oxide nanoparticles with adjustable morphology and their photocatalytic performances, *Carbohydr. Polym.*, 2021, **259**, 1–61.

47 A. Tanwar, P. Date and D. Ottoor, ZnO NPs incorporated gelatin grafted polyacrylamide hydrogel nanocomposite for controlled release of ciprofloxacin, *Colloids Interface Sci. Commun.*, 2021, **42**, 100413.

48 H. T. Draviana, I. Fitriannisa, M. Khafid, D. I. Krisnawati, L. C.-H. Widodo, Y.-J. Fan and T.-R. Kuo, Size and charge effects of metal nanoclusters on antibacterial mechanisms, *J. Nanobiotechnol.*, 2023, **21**, 428, DOI: 10.1186/s12951-023-02208-3.

49 L. Salvioni, E. Galbiati, V. Collico, G. Alessio, S. Avvakumova, F. Corsi, P. Tortora, D. Prosperi and M. Colombo, Negatively charged silver nanoparticles with potent antibacterial activity and reduced toxicity for pharmaceutical preparations, *Int. J. Nanomed.*, 2017, **12**, 2517–2530, DOI: 10.2147/IJN.S127799.

50 K. V. Dhandapani, D. Anbumani, A. D. Gandhi, P. Annamalai, B. S. Muthuvenkatachalam, P. Kavitha and B. Ranganathan, Green route for the synthesis of zinc oxide nanoparticles from Melia azedarach leaf extract and evaluation of their antioxidant and antibacterial activities, *Biocatal. Agric. Biotechnol.*, 2020, **24**, 101517, DOI: 10.1016/j.bcab.2020.101517.

51 S. Jiang, K. Lin and M. Cai, ZnO nanomaterials: current advancements in antibacterial mechanisms and applications, *Front. Chem.*, 2020, **8**, 580, DOI: 10.3389/fchem.2020.00580.

52 H. Agarwal, S. Menon, S. V. Kumar and S. Rajeshkumar, Mechanistic study on antibacterial action of zinc oxide nanoparticles synthesized using green route, *Chem.-Biol. Interact.*, 2018, **286**, 60–70, DOI: 10.1016/j.cbi.2018.03.008.

53 L. Wang, C. Hu and L. Shao, The antimicrobial activity of nanoparticles: present situation and prospects for the future, *Int. J. Nanomed.*, 2017, **12**, 1227–1249, DOI: 10.2147/IJN.S121956.

54 S. A. Amur, N. A. Soomro, Q. Khuhro, Y. Wei, H. Liang and Q. Yuan, Encapsulation of natural drug gentiopicroside into zinc based Zeolitic Imidazolate Frameworks (ZIF-8): *in vitro* drug release and improved antibacterial activity, *J. Drug Deliv. Sci. Technol.*, 2023, **84**, 104530, DOI: 10.1016/j.jddst.2023.104530.

55 M. Biernat, A. Sylla, K. A. Stępień, J. Giebułtowicz, L. Ciołek, P. Szterner, P. Tymowicz-Grzyb, B. Kózka and D. Olczak-Kowalczyk, Multi-Antibiotic Porous Systems for Tailored Drug Delivery in Dentistry: Formulation Strategy, Physicochemical Properties, and Release, *Pharmaceutics*, 2026, **18**(4), 409, DOI: 10.3390/pharmaceutics18040409.

56 M. Ullah, J. Lee, N. Hasan, M. L. Hakim, D. Kwak, H. Kim, E. Lee, J. Ahn, B. Mun, E. H. Lee, *et al.*, Clindamycin-Loaded Polyhydroxyalkanoate Nanoparticles for the Treatment of Methicillin-Resistant Staphylococcus aureus-Infected Wounds, *Pharmaceutics*, 2024, **16**, 1315, DOI: 10.3390/pharmaceutics16101315.

57 S. M. Mahgoub, E. A. Mohamed, S. A. Abdel Aziz, A. A. Allam, H. E. Alfassam, R. Shafei and R. Mahmoud, Synergistic potential of clindamycin hydrochloride loaded on zinc

oxide nanoparticles: a novel approach to combat multidrug-resistant infections, *Sci. Rep.*, 2025, **15**, 44665.

58 S. A. Habeeb, A. H. Hammadi, D. Abed and L. F. Al-Jibouri, Green synthesis of metronidazole or clindamycin-loaded hexagonal zinc oxide nanoparticles from Ziziphus extracts and its antibacterial activity, *Pharmacia*, 2022, **69**(3), 855–864, DOI: 10.3897/pharmacia.69.e91057.

59 S. R. Shah, A. M. Tatara, J. Lam, S. Lu, D. W. Scott, G. N. Bennett, J. J. J. P. van den Beucken, J. A. Jansen, M. E. Wong and A. G. Mikos, Polymer-Based Local Antibiotic Delivery for Prevention of Polymicrobial Infection in Contaminated Mandibular Implants, *ACS Biomater. Sci. Eng.*, 2016, **2**(4), 558–566.

60 S. H. Ismail, A. Hamdy, T. A. Ismail, H. H. Mahboub, W. H. Mahmoud and W. M. Daoush, Synthesis and Characterization of Antibacterial Carbopol/ZnO Hybrid Nanoparticles Gel, *Crystals*, 2021, **11**(9), 1092, DOI: 10.3390/cryst11091092.